Title

Expression, purification and structural properties of ABC transporter ABCA4 and its individual domains.

Authors

Tsybovsky, Yaroslav
Palczewski, Krzysztof

Publication Date

2014-05-01

DOI

10.1016/j.pep.2014.02.010

Peer reviewed

Published in final edited form as:
Protein Expr Purif. 2014 May ; 97: 50–60. doi:10.1016/j.pep.2014.02.010.

Expression, purification and structural properties of ABC transporter ABCA4 and its individual domains

Yaroslav Tsybovsky and **Krzysztof Palczewski**[*]
Department of Pharmacology, School of Medicine, Case Western Reserve University, 10900 Euclid Ave, Cleveland, Ohio 44106, USA

Abstract

ABCA4 is a member of the A subfamily of ATP-binding cassette transporters that consists of large integral membrane proteins implicated in inherited human diseases. ABCA4 assists in the clearance of *N*-retinylidene-phosphatidylethanolamine, a potentially toxic by-product of the visual cycle formed in photoreceptors during light perception. Structural and functional studies of this protein have been hindered by its large size, membrane association, and domain complexity. Although mammalian, insect and bacterial systems have been used for expression of ABCA4 and its individual domains, the structural relevance of resulting proteins to the native transporter has yet to be established. We produced soluble domains of ABCA4 in *E. coli* and *S. cerevisiae* and the full-length transporter in HEK293 cells. Electron microscopy and size exclusion chromatography were used to assess the conformational homogeneity and structure of these proteins. We found that isolated ABCA4 domains formed large, heterogeneous oligomers cross-linked with non-specific disulphide bonds. Incomplete folding of cytoplasmic domain 2 was proposed based on fluorescence spectroscopy results. In contrast, full-length human ABCA4 produced in mammalian cells was found structurally equivalent to the native protein obtained from bovine photoreceptors. These findings offer recombinantly expressed full-length ABCA4 as an appropriate object for future detailed structural and functional characterization.

Keywords

ABCA4; ABCA subfamily; ABC transporter; heterologous expression; monodispersity; electron microscopy

INTRODUCTION

ATP-binding cassette (ABC) transporters comprise one of the largest and most ancient protein superfamilies, with representatives found in all kingdoms of life [1]. They use the energy of ATP hydrolysis to selectively transport various compounds across biological

[*]Corresponding author: Krzysztof Palczewski, kxp65@case.edu, Phone: +1 216 368 4497.

membranes. This universal function dictates a common general architecture, including the presence of two nucleotide- binding domains (NBDs) responsible for nucleotide cleavage and two transmembrane domains (TMDs) that form a path for substrate translocation [2]. In accordance with their high substrate diversity, however, ABC transporters differ significantly with respect to primary structure, molecular organization, and size. In particular, their constituent elements can be incorporated into a single polypeptide chain (full transporters), organized in two separate chains (half transporters) or be expressed as independent proteins that assemble to form a functional transporter. Additional components can be present in the form of substrate-binding proteins and regulatory domains. Significant sequence similarities among unrelated ABC transporters are usually detected only in their NBDs.

Among the seven mammalian ABC subfamilies (named A through G), ABCA contains the largest ABC transporters known to date. Thus, five out of twelve ABCA members, ABCA1, ABCA2, ABCA4, ABCA12 and ABCA13 exceed the molecular weight (MW) of 250 kDa. Mutations in several human ABCA transporters have been linked to severe health disorders, including a disruption in cholesterol homeostasis known as Tangier disease (ABCA1), pulmonary surfactant deficiency in new-borns (ABCA3), a number of blinding retinal dystrophies such as Stargardt disease [3, 4] and cone-rod dystrophy [5] (ABCA4), and the fatal skin disease, harlequin type ichthyosis (ABCA12) [6–8].

ABCA4 is a member of the A subfamily predominantly localized to the outer segments (OS) of photoreceptors, specialized neurons found in the retina (Figure 1A) [9]. Light perception in vertebrates is associated with continuous renewal of the visual pigment chromophore, 11-*cis*-retinal, in a process known as the retinoid or visual cycle [10, 11]. High chemical reactivity of all-*trans*-retinal (ATR), the product of light-induced isomerisation of 11-*cis*-retinal, can lead to severe retinal pathology [12]. A substantial body of evidence suggests that ABCA4 is involved in the clearance of ATR from photoreceptors by transporting *N*-retinylidene-phosphatidylethanolamine (*N*-retinylidene-PE), the reversible Schiff base conjugate between ATR and phosphatidylethanolamine, from the luminal to the cytoplasmic side of disc membranes in photoreceptor OS [13–17]. Hundreds of mutations in the *ABCA4* gene have been linked to visual diseases in humans [9].

The membrane topology of ABCA4 was established based on computational prediction of transmembrane helices and experimental determination of glycosylation and phosphorylation sites [18, 19] (Figure 1B). Each of the two homologous but non-identical halves of this full transporter starts with a transmembrane helix followed by a glycosylated exocytoplasmic domain (ECD). The ~600 residue-long ECD1 and ~280 residue-long ECD2 do not show significant homology to any protein sequence outside of the ABCA subfamily. The ECD is followed by five more transmembrane helices that complete the TMD. The subsequent cytoplasmic domain (CD), although often called an NBD, is substantially extended compared to the canonical NBD sequence. In particular, only the N-terminal part of CD1 constituting about 50% of its primary structure is represented by the NBD, whereas the C-terminal part has no sequence homologues and has not been functionally characterized. The presence of at least five phosphorylation sites in the regions flanking NBD1 within CD1 (Figure 1B) suggests a regulatory role for this moiety [19]. Similarly,

NBD2 occupies only 60% of CD2. This general membrane topology is shared by ABCA1 [20] and likely other members of the ABCA subfamily.

Despite considerable effort inspired by the physiological importance of ABCA4 for maintaining normal vision, structural studies of this transporter have been hampered by its complexity, limited availability and transmembrane nature. In the absence of direct structural information, many related properties of ABCA4 and other members of subfamily A have been inferred from biochemical and biophysical characterization of the full-length protein expressed in mammalian cells [14, 17–19, 21–23] or individual domains produced in bacteria in the soluble form or refolded from inclusion bodies (IB) [24–30]. Whether these recombinant analogues sufficiently recapitulate the conformation and properties of native ABCA4 could not be tested at that time [9]. We recently used electron microscopy (EM) and single particle analysis to determine ligand-free and ATP-bound structures of native ABCA4 purified from bovine retinas to a resolution of 18–19 Å (Figure 1C) [31]. These structures provided a physiologically relevant reference that allowed us to investigate the qualities of recombinantly expressed ABCA4 and its fragments. To allow for a future structural analysis of ABCA4 mutants found in patients suffering from retinal degeneration, we expressed and purified full-length recombinant ABCA4 and its individual domains. We then used EM and biochemical tools to characterize the conformation of these proteins. We found that ABCA4 fragments produced in *E. coli* and yeast formed non-native high-order oligomers non-specifically cross-linked with disulphide bonds. A more detailed characterization of CD2 suggested incomplete folding. In contrast, human ABCA4 expressed in HEK293 cells was structurally equivalent to the bovine protein obtained from its native source, at least at the currently achievable resolution.

MATERIALS AND METHODS

Materials

The pCEP4-ABCA4 plasmid encoding untagged full-length human ABCA4 was a kind gift of Dr. Robert S. Molday (University of British Columbia). The YEpHIS plasmid was generously provided by Dr. Vera Moiseenkova-Bell (Case Western Reserve University). The monoclonal anti-His antibody was purchased from GeneScript. Bovine eyes were obtained from a local slaughterhouse.

Molecular cloning and site-directed mutagenesis

Total RNA was purified from one fresh bovine retina with RiboPure Kit (Life Technologies) according to the manufacturer's instructions. cDNA was synthesized with the SuperScript III First-Strand Synthesis System (Life Technologies) using oligo(dT) primers. For *E. coli* expression, cDNA regions encoding the ABCA4 fragments of interest were amplified by PCR and cloned into the pET-45b(+) vector (Novagen) or the pGEX vector (GE Healthcare, GST-CD2 construct only). All pET-45b(+) constructs carried an N-terminal tag of 6 His residues connected to the protein through a short linker ('VGTG' for his-ECD1, his-CD2, his-CD2short, his-CD2-strep and his-NBD2; 'VGT' for his-ECD2 and his-CD1), whereas the his-CD2-strep construct additionally carried a C-terminal Strep-tag II ('WSHPQFEK'). For yeast expression, CD2 and ECD2 domains each carrying a C-terminal 1d4

immunoaffinity tag ('TETSQVAPA') were cloned into the YEpHIS plasmid using SpeI and MluI restriction sites [32, 33]. Mutations were introduced with the QuikChange site-directed mutagenesis kit (Agilent Technologies). All constructs were verified by DNA sequencing. Table 1 lists ABCA4 fragments used in this study.

Bacterial expression, purification and refolding of ABCA4 fragments

Recombinant bovine ABCA4 fragments were produced in *E. coli* strains BL21 Star (DE3) or Origami B (DE3) (Novagen). Cells were grown in the presence of 50 μg/ml ampicillin at 37°C until reaching an OD_{600} of 0.6. The temperature was reduced to 24°C and protein expression was induced by addition of 0.1 mM isopropyl β-D-1-thiogalactopyranoside (IPTG). For production of target proteins in the form of inclusion bodies (IB), the temperature was maintained at 37°C after induction with 0.5 mM IPTG. Cells were pelleted after 5 h of expression, resuspended in 50 mM Tris-HCl, pH 8.1, 250 mM NaCl, 1 mM β-mercaptoethanol (buffer A) supplemented with Complete EDTA-free Protein Inhibitor Cocktail (Roche) and disintegrated by sonication. The insoluble fraction was separated by centrifugation at 35,000 g for 30 min at 4 °C.

To purify soluble his-CD2-strep from 1 L of cell culture, the soluble fraction of cell lysate was loaded on a 2 ml Ni-NTA (Qiagen) column pre-equilibrated with buffer A at 4 °C. The resin was sequentially washed with buffer A containing 0 and 35 mM imidazole, and bound proteins were eluted with 200 mM imidazole in the same buffer. The eluate was applied to a 1 ml Strep-Tactin column (IBA GmbH) pre-equilibrated with 100 mM Tris-HCl, pH 8.1, 150 mM NaCl and 1 mM dithiothreitol (DTT) (buffer B). This column was washed with 20 column volumes of buffer B, and bound proteins were eluted with the same buffer supplemented with 5 mM desthiobiotin. The eluted protein was subjected to size exclusion chromatography (SEC) or dialysed against buffer containing 20 mM Bis-Tris propane (BTP), pH 7.5, 100 mM NaCl and 1 mM DTT (buffer C)

To purify ABCA4 fragments from bacterial IB, the cell lysate pellet was resuspended in 100 mM Tris-HCl, pH 8.1, 100 mM NaCl, 1 mM β-mercaptoethanol (buffer D) containing 6 M guanidine hydrochloride (Gdn) and incubated at RT for 2 h with rocking. The solution was cleared by centrifugation and loaded on a 2 ml Ni-NTA column pre-equilibrated with buffer D containing 5 M urea. The column was washed with the same buffer supplemented with 30 mM imidazole followed by elution with buffer D in the presence of 5 M urea and 300 mM imidazole. Refolding was accomplished by an overnight dialysis against buffer D followed by another dialysis against buffer C. Alternatively, a stepwise refolding scheme was applied with the urea concentration reduced to 4 M, 2 M, 1 M and 0 M by separate dialysis steps. In another approach, the urea concentration was reduced to 0.5 M by diluting the sample prior to the dialysis against buffer C. For consistency, refolded his-CD2-strep was additionally purified by Strep-Tactin affinity chromatography as described for soluble his-CD2-strep.

Expression of ECD2 and CD2 in yeast

S. cerevisiae strain BJ5457 was transformed with YEpHIS plasmids encoding ECD2 or CD2 domains of ABCA4 following the protocol described earlier [34]. Transformed colonies were grown in 0.5 l of SD media lacking leucine (SD Medium-Leu, MP Biomedicals) in the

presence of 10% glycerol for 36 h at 30 °C with constant agitation (225 rpm). The cells were pelleted and resuspended in 25 ml of the ice-cold buffer containing 25 mM Tris-HCl, pH 8.1, 300 mM sucrose, 5 mM EDTA and yeast protease inhibitor cocktail (Sigma). Vortexing in the presence of glass beads was used to lyse the cells. Insoluble material was removed by centrifugation, and the supernatant was used for analysis.

Expression and purification of full-length human ABCA4

HEK293 cells were maintained in HyClone DMEM medium supplemented with 10% fetal bovine serum, 50 units/ml penicillin and 50 μg/ml streptomycin. Adherent cells (one 75 mm^2 flask) were transfected at 80% confluence with 20 μg of pCEP4-ABCA4 by using the X-tremeGENE 9 DNA transfection reagent (Roche). After 48 h, cells were washed in PBS, harvested by scraping and pelleted. All the following procedures were done at 4 °C or on ice. The pellet was solubilized with 1 ml of 20 mM BTP, pH 7.5, 10% glycerol, 150 mM NaCl, 3 mM $MgCl_2$, 1 mM DTT, 2 mg/ml porcine brain polar lipids (Avanti Polar Lipids, Alabaster, AL, USA) and 25 mM n-dodecyl-β-D-maltopyranoside (DDM) for 1 h, followed by centrifugation at 100 000 g for 15 min. The soluble fraction was incubated for 1.5 h with 0.1 ml of the Rim3F4 anti-ABCA4 monoclonal antibody [35] conjugated to agarose. The resin was washed 6 times with 20 mM BTP, pH 7.5, 10% glycerol, 150 mM NaCl, 1 mM DTT and 0.5 mM DDM. ABCA4 was eluted by incubation for 15 min with 0.2 ml of the same buffer supplemented with 0.5 mg/ml crude YDLPLHPRT peptide. Next, the eluate was supplemented with 0.1 mM $CaCl_2$ and 0.1 mM $MnCl_2$ and incubated with 0.1 ml of agarose-bound *Galanthus nivalis* lectin (GNL, Vector Laboratories, Burlingame, CA, USA) for 1 h. After 5 washes with 0.5 ml of the above buffer, the resin was incubated for 1 h with the same buffer containing 0.2 mg/ml Amphipol A8-35 (Affymetrix, Santa Clara, CA, USA) to allow the substitution of Amphipol for the detergent. This was followed by ten 0.5 ml washes with the buffer devoid of DDM and Amphipol. The bound proteins were then eluted with 0.5 ml of 20 mM BTP, pH 7.5, 10% glycerol, 150 mM NaCl, 1 mM DTT supplemented with 0.5 M methyl α-D-mannopyranoside. Finally, methyl α-D-mannopyranoside was removed using a desalting column.

Size exclusion chromatography

SEC was done at 4 °C by using a 30 cm-long Superose 6 GL column with a diameter of 1 cm (GE Healthcare) at a flow rate of 0.3 ml/min. Sample volumes varied from 0.1–0.5 ml. Larger samples (5 ml) were separated on a 60 cm-long HiPrep Sephacryl S-300 column (GE Healthcare) with a diameter of 2.6 cm at a flow rate of 1.0 ml/min. Columns were equilibrated with buffer C, which in some experiments was supplemented with 10% glycerol or 2 mM DDM.

Intrinsic and ANS fluorescence

Measurements were done with a PerkinElmer LS-55 fluorescence spectrometer. The protein concentration was 25 μg/ml. Intrinsic tryptophan fluorescence was excited at 295 nm and recorded between 310–400 nm. 1-anilinonaphthalene-8-sulfonate (ANS) fluorescence was excited at 360 nm and recorded between 400–560 nm. The ANS-to-protein molar ratio was 20:1. All spectra were corrected for the fluorescence of their corresponding buffers.

Transmission EM and single particle analysis

Protein samples diluted to 1–10 μg/ml were applied to glow-discharged, carbon film-coated copper grids and incubated for 2 min at RT. The grids were blotted and washed in two droplets of distilled water. After blotting, grids were stained with 1% (w/v) uranyl acetate. Micrographs were recorded with either a FEI Tecnai T12 or F20 microscopes (FEI, Eindhoven, Netherlands) operated at 100 or 200 kV, respectively, and equipped with CCDs. The magnifications were 69,400 (T12) and 70,400 (F20). Particles were picked manually by using e2boxer from the EMAN2 software package [36]. Reference-free 2D class averages were calculated with SPIDER [37] by using the rotationally invariant K-means reference-free alignment and classification algorithm [38].

ATPase activity assays

For ATPase activity measurements of full-length ABCA4, the protein was purified as described above except that the DDM detergent was replaced with 18 mM CHAPS for the solubilization step and 10 mM for all other steps. All purification buffers contained 1 mg/ml brain polar lipid. ABCA4 was eluted from the immunoaffinity column with 0.5 mg/ml of the epitope peptide in the absence of Amphipol. The protein was reconstituted in lipid vesicles by mixing 0.5 ml of the ABCA4 sample with 2 ml of 20 mM BTP, pH 7.5, 10% glycerol, 150 mM NaCl, 3 mM $MgCl_2$, 2 mM DTT, 10 mM CHAPS, 1 mg/ml brain polar lipid followed by a dialysis at 4 °C against 1 l of the same buffer containing no detergent and no lipid. The basal and ATR-stimulated activities were measured after 24 h by monitoring the hydrolysis of [γ-^{33}P]ATP in the absence or presence of 0.1 mM ATR, respectively, as described by us previously [19].

The ATPase activity of his-CD2-strep was measured using two different approaches. In the first approach, the purified protein was supplemented with 1 mM $MgCl_2$, and the ATPase reaction was initiated by addition of 10 μl of 10x ATP stock containing 1 mM ATP and 1 μCi of [γ-^{33}P]ATP to 90 μl of the sample followed by an incubation for 30 min at 37 °C. The reaction was stopped by mixing with 1 ml of 10% charcoal in 10 mM HCl. Radioactivity of the supernatant was then counted after centrifugation [19]. In the second approach, a 9 μl sample of purified his-CD2-strep was mixed with 1 μl of solution containing 1 mM ATP, 1 μCi of [α-^{32}P]ATP and 10 mM $MgCl_2$. After 30 min incubation at 37 °C, the samples were placed on ice and EDTA was added to the final concentration of 10 mM to stop the reaction. 1 μl of the reaction mixture was spotted onto a polyethyleneimine cellulose plate (Sigma) and chromatographed in 0.7 M KH_2PO_4. The plate was exposed to a storage phosphor screen and scanned with a Typhoon 9410 scanner (GE Healthcare).

Other methods

Sequence alignments were done with Clustal Omega [39].

RESULTS

Individual ABCA4 domains expressed in E. coli form high-MW, irregular oligomers

Based on the membrane topology of ABCA4 (Fig. 1B), we prepared eight constructs encoding regions that likely correspond to its soluble domains. These fragments included

His-tagged ECD1, ECD2, CD1, CD2, CD2short, NBD2 and a fusion of glutathione S-transferase (GST) with CD2 (Table 1). An additional his-CD2-strep construct also carried a C-terminal Strep-tag II to simplify purification. Strong protein expression was detected in all cases (see Figure 2A for an example), although the yield of soluble protein differed among constructs (Table 1). To characterize individual ABCA4 domains, we first isolated his-CD2-strep from the soluble fraction of a cell lysate. The purification protocol consisted of Ni-NTA and Strep-Tactin affinity chromatography steps (Figure 2B), with a typical yield of 0.5–1.0 mg of his-CD2-strep from 1 l of cell culture. As indicated by the manufacturer of the Strep-Tactin resin, “The soluble part of the *E. coli* total cell extract contains no proteins beyond the nearly irreversibly binding biotin carboxyl carrier protein (BCCP) which bind significantly to the *Strep*-Tactin column” (‘Expression and purification of proteins using *Strep*-tag or Twin-Strep-tag’, IBA Solutions For Life Sciences; available at http://www.iba-lifesciences.com/technical-support.html as of January 28, 2014). We confirmed the validity of this statement by passing the soluble part of *E. coli* cell lysate obtained from the culture expressing his-CD2 without the Strep-tag (data not shown). Despite this high specificity of the Strep-Tactin chromatography, a number of contaminating proteins were observed in the elution fractions in addition to the major band (Fig. 2B), suggesting their specific or non-specific interaction with his-CD2-strep. The SEC profile of the purified protein showed a broad peak covering MWs from about 150 kDa to the exclusion limit of the Superose 6 matrix (~5 MDa), with little or no monomer present (Figure 2C, top). We then examined these samples by negative-stain EM, an excellent tool for analysis of protein conformational homogeneity [40]. The protein was adsorbed on a carbon-coated grid and stained with uranyl acetate. Visualization with an electron microscope (Figure 2C, bottom) revealed non-specific aggregates of variable sizes (note that the length of the white bar on the micrograph corresponds to 20 nm, the largest dimension of full-length native ABCA4 [31]).

For comparison, we then obtained the same his-CD2-strep fragment by refolding from IB. The sediment of the cell lysate was solubilized with Gdn and subjected to Ni-NTA chromatography under denaturing conditions. The protein then was refolded before the Strep-Tactin purification step (see Materials and Methods). This protocol typically yielded 10–15 mg of pure his-CD2-strep from 1 l of cell culture. Contaminating proteins were not observed in Strep-Tactin elution fractions (Figure 2D, top, inset), presumably because they were detached by Gdn and separated during the Ni-NTA step. The SEC profile was similar to that obtained for his-CD2-strep from the soluble fraction, but the broad peak was further shifted towards high MWs (Figure 2D, top). In agreement with this observation, large irregular aggregates were observed in EM images (Figure 2C, bottom). his-CD2-strep samples obtained with three different refolding approaches, including one-step and multi-step dialysis and rapid dilution, demonstrated identical SEC profiles. We further determined that the presence of detergent (2 mM DDM) or 10% glycerol (essential for keeping full-length ABCA4 in solution) during refolding did not alter the non-specific oligomerization of CD2 as assessed by SEC (data not shown).

We then used SEC and EM to determine the oligomeric state of ECD2 and CD1, the remaining two domains of ABCA4 that were obtained in a soluble form by refolding from IB after purification with Ni-NTA chromatography. SEC of the 280 residue-long his-ECD2

fragment revealed a broad peak centred at about 500–600 kDa (Figure 3A). In agreement with this, large oligomers of variable shapes were detected by EM. Similarly, the chromatographic profile and EM images of his-CD1 indicated formation of high-MW, heterogeneous oligomers (Figure 3B). Notably, despite massive oligomerization, ECD2, CD1 and CD2 domains remained soluble at concentrations as high as 5–10 mg/ml. Protein concentrations within the 0.1–10 mg/ml range did not influence the chromatogram profiles.

Bacterial expression of ABCA4 domains results in formation of non-specific disulphide bonds

Bovine ABCA4 contains a total of 42 Cys residues (*versus* 43 in the human orthologue) of which 8, 5, 12 and 7 are located in ECD1, ECD2, CD1 and CD2, respectively. It is not currently known if disulphide bonds are present in ABCA4, except for some evidence in favour of such a linkage between ECD1 and ECD2 [18]. Failure to form native disulphide bonds or the presence of aberrant disulphides could be the reason for the observed oligomerization of the individual ABCA4 domains. Thus, we used SDS-PAGE analysis of cell lysates in the presence and absence of a reducing agent to probe for non-specific disulphide linkages. This analysis revealed high MW bands and smears (Figure 4A–B). In the case of CD1 and all CD2 constructs, multiple bands corresponding to the protein monomer also were detected. Combined, these findings indicate formation of aberrant inter-molecular as well as intra-molecular disulphide bridges in ABCA4 fragments expressed in bacteria. Noteworthy, these non-specific bonds were equally present in proteins expressed in BL21 and Origami B cells that provide a better environment for disulphide bond formation in proteins (data not shown).

ECD2 and CD2 fragments expressed in yeast form non-specific disulphide bonds

To verify if the tendency to form non-specific disulphide bridges can be overcome by a eukaryotic expression system, we produced ECD2 and CD2 fragments of ABCA4 in *S. cerevisiae* using an episomal vector with constitutive promoter PMA1. The corresponding proteins, ECD2-1d4 and CD2-1d4, were detected by Western blot with 1d4 monoclonal antibody in soluble fractions of cell lysates (Figure 5). We found that in the absence of the reducing agent, ECD2-1d4 (Figure 5A) and CD2-1d4 (Figure 5B) formed multiple high-MW species, indicating non-specific cross-linking via disulphides bonds.

Replacement of Cys residues does not prevent oligomerization of CD2

We chose his-CD2 for a more detailed characterization. The seven Cys residues of CD2 are located in the NBD. These are invariant among the ABCA4 orthologues, but show variable degrees of conservation within the ABCA subfamily (Figure 6A) and are generally not conserved among the members of the superfamily of ABC transporters. To determine if aberrant disulphide bonds were the driving force of the non-specific oligomerization of his-CD2, we used mutagenesis to replace these Cys residues with Ser residues. Because an exhaustive search through all possible combinations would be impractical due to the necessity of obtaining 127 mutants, the Cys residues were instead replaced sequentially. The resulting mutants containing from six down to two Cys showed unaltered expression levels and were refolded after purification from IB (Figure 6B, left) except for the C2135S

mutation construct that led to protein precipitation. As expected, gradual removal of Cys residues decreased the tendency to form non-specific inter-molecular disulphide bonds (Figure 6B, right). Furthermore, a single SDS-PAGE band representing the protein monomer was observed after introducing the C2015S mutation, indicating possible involvement of C2015 in an intra-molecular disulphide bridge.

Importantly, the observed reduction in chemical heterogeneity did not alleviate the tendency of his-CD2 to form large oligomers as determined by SEC (Figure 6C). Furthermore, the tryptophan fluorescence spectra of refolded wild type (WT) his-CD2 and the mutant devoid of five out of seven Cys were found to be identical, indicating the lack of gross conformational changes (Figure 6D, left). Thus, formation of non-specific disulphide bridges is likely to be a consequence rather than the reason for the oligomerization. The emission maximum located at 335 nm and the red shift observed upon denaturation suggested that the two fluorescent Trp residues present in the NBD of CD2 are protected from quenching by the solvent as is usually observed in compact globular proteins. However, a blue shift in the emission spectrum of ANS together with a significant increase in its fluorescence intensity (Figure 6D, right) indicated binding of this hydrophobic dye to both WT and mutated CD2 under normal but not denaturing conditions. This suggests the presence of solvent-exposed hydrophobic regions, which are typically observed in partially unfolded conformational states.

ATPase activity of CD2

The ATPase hydrolysis rate of his-CD2-strep purified from the soluble fraction of cell lysate was found to be 19.5±4.3 nmol(ATP)/mg(protein)/min. Our concern, however, was the presence of contaminating proteins bound to his-CD2-strep (Figure 2B). To evaluate the contribution of these contaminants, we generated an inactive K1978M mutant [17] of his-CD2-strep and purified it by using exactly the same protocol, which resulted in similar protein yield and purity (data not shown). The ATPase activity of these protein preparations, measured by two different approaches (see Materials and Methods), was found to be identical to that of unmutated his-CD2-strep. This suggests that contaminating proteins are mainly responsible for the ATPase activity in the samples of his-CD2-strep.

Full-length recombinant ABCA4 is structurally equivalent to ABCA4 purified from a native source

The untagged, full-length human ABCA4 protein (89% sequence identity with the bovine orthologue) was transiently expressed in mammalian HEK293 cells. The commonly used protocol for purification of ABCA4 utilizes the immobilized Rim3F4 monoclonal antibody [13, 35] (Figure 7A). In order to obtain high-quality micrographs of ABCA4 for structural studies by single particle analysis, the detergent used in solubilization and purification steps must be exchanged for Amphipol A8-35, an amphipathic polyacrylate-based polymer capable of binding to transmembrane helices and stabilizing membrane proteins [41]. Such a reconstitution, which allows to omit the detergent from sample buffer, was needed for successful structural analysis of native bovine ABCA4 [31]. However, we found that addition of Amphipol to ABCA4 that was bound to the immunoaffinity resin elutes the protein in a mixture of detergent and Amphipol (data not shown), precluding structural

studies. A possible explanation for this behaviour is that the antibody epitope is located close to the trans-membrane region, which results in a competition between the antibody and Amphipol for binding to the protein. To avoid this problem, we introduced a second purification step. We showed previously that oligosaccharides decorating the ECDs of native ABCA4 are rich in α-linked mannose [19], which results in binding to the agarose-conjugated lectin from *Galanthus nivalis* (GNL) [31]. The recombinantly expressed protein retained this property, which allowed development of the following two-step purification scheme. First, ABCA4 was purified using the conventional immunoaffinity approach in the presence of DDM detergent. Second, the resulting protein was bound to the GNL resin, DDM was replaced with Amphipol, and the protein-Amphipol complex was eluted with the competing sugar. This new isolation strategy also increased the protein purity (Figure 7A), facilitating unambiguous structural analysis by EM. A typical protein yield was about 0.5 μg of pure ABCA4 from a 75 cm^2 flask, with significant variations expected for a transient expression system. The basal ATP hydrolysis rate of ABCA4 after reconstitution in brain polar lipid vesicles was 75±4 nmol(ATP)/mg(protein)/min. Addition of 0.1 mM ATR stimulated this activity about twice, to 143±20 nmol(ATP)/mg(protein)/min. These values are in good agreement with previously published data [14].

EM images revealed uniformly distributed particles of the expected size (~20 nm in the longest dimension) and typical elongated shape, with only a small fraction of aggregates present (Figure 7B). A total of 891 particles were collected from 30 micrographs and used to obtain two-dimensional (2D) class averages (Figure 7C). These revealed distinctive features that we observed earlier in ABCA4 purified from native bovine eyes, including the ‘ice cream cone’-like shape of the molecule with an elongated ‘handle’ representing the ECDs and the ‘head’ encapsulating the CDs and Amphipol-embedded TMDs [31] (Figure 7C, 1B). The apparent quality of these 2D class averages was comparable to or better than that of 2D class averages formed from 891 particles randomly selected from the dataset previously used to determine the structure of native bovine ABCA4 [31] (Figure 7C). These results strongly suggest a structural identity of recombinant ABCA4 expressed in mammalian cells to the protein obtained from a native source.

DISCUSSION

Large membrane proteins represent especially challenging targets for structural studies. With several members implicated in various severe human diseases, the A subclass of mammalian ABC transporters can serve as an exemplary protein family still lacking sufficient structural description despite significant advances in biochemical and clinical characterization [7, 42, 43]. The intricate membrane topology, multiple posttranslational modifications and unusual size (Figure 1B) dictate the predominant choice of mammalian expression systems for production of these proteins, as utilized in a number of studies (see [14, 17–23, 44, 45] for some examples). Alternatively, the presence of large regions apparently capable of forming soluble individual domains (Figure 1B) prompted other researchers to produce these as isolated proteins in *E. coli*, an attractive host that facilitates obtaining large amounts of a target protein at a low cost [24–30, 46]. Here we used the EM structure of bovine ABCA4 purified from its native source [31] as a reference to investigate

the properties of its recombinant fragments produced in bacteria as well as those of full-length human orthologue expressed in mammalian HEK293 cells.

ECD1, ECD2, CD1 and CD2 fragments of bovine ABCA4 expressed in *E. coli* showed a tendency to form non-native high-order oligomers. Thus, broad SEC peaks corresponding to an average MW on the order of 1 MDa were obtained for his-CD2-strep isolated from the soluble fraction of cell lysate (Figure 2C) as well as for his-ECD2 (Figure 3A), his-CD1 (Figure 3B) and his-CD2 (Figure 2D) refolded from bacterial IB. In agreement with this finding, visualization of these proteins with EM revealed structurally heterogeneous particles with sizes far exceeding the longest dimension of native full-length bovine ABCA4 [31] (Figures 2C, 2D, 3A, 3B). These irregular soluble aggregates were observed in conjunction with non-specific inter-molecular and intra-molecular (in the case of CDs) disulphide bonds revealed by non-reducing SDS-PAGE (Figure 4, 5). Production of ECD2 and CD2 fragments in yeast did not alleviate this cross-linking problem. Notably, sequential replacement of Cys residues with Ser residues in his-CD2 reduced this chemical cross-linking (Figure 6B) but did not influence the propensity to self-associate (Figure 6C), suggesting that formation of inter-molecular disulphide bonds is likely to be a secondary event. Furthermore, although intrinsic fluorescence studies suggest a compact overall conformation of CD2 with tryptophan residues shielded from the solvent, the observed binding of ANS under physiological conditions indicates the presence of solvent-accessible hydrophobic regions (Figure 6D). This combination is typically observed in partially unfolded proteins [47–50]. Thus it is possible that incomplete folding of the protein monomer initiates oligomerization of CD2.

It can be argued that the non-native conformation of recombinant ABCA4 fragments is an intrinsic property of these proteins originating from the structural organization of the full-length transporter (Figure 1). In particular, in the EM structure of native ABCA4 the two ECDs form a single structural unit [31] (Figure 1C). This observation is in line with the presence of at least one disulphide bridge between these two domains, as suggested by an earlier study [18]. Similarly, the CDs were found to be tightly associated, with no complete separation observed upon addition of an ATP analogue [31]. These interactions may be critical for correct folding. Furthermore, the localization of endogenous ABCA4 in the rims of disk membranes of photoreceptor OS [51, 52] creates a unique environment for ECDs, which are likely to be tightly surrounded by a curved lipid bilayer [31] (Figure 1A). In addition, ECD1 is glycosylated at three and four positions, respectively, in bovine and human ABCA4, whereas ECD2 has four attached polysaccharides [18, 19]. It is known that protein glycosylation can be important for attaining the native conformation [53]. In its turn, CD1 was shown to be phosphorylated [19]. All these properties reduce the probability of correct folding of isolated ABCA4 domains expressed in bacteria.

Several published studies have described various characteristics of individual CD1, CD2 and ECD2 fragments of human ABCA4 produced in *E. coli*, with N-terminal S-tags used for purification. In particular, it was shown that CD1 and CD2 have ATPase activity that can be altered by introducing naturally occurring mutations [24–26, 29]. Furthermore, functional interactions of CD1 and CD2 were proposed that regulate their activity [27]. Finally, two recent studies suggested that ECD2 and CD1 are capable of binding ATR and 11-*cis*-retinal,

respectively [28, 30]. The last three papers relied on fluorescence anisotropy, a technique that is critically dependent on sample monodispersity. Curiously, none of these published studies reported any data about the oligomerization state or conformational homogeneity of the corresponding ABCA4 fragments, with protein 'homogeneity' assessed solely with reducing SDS-PAGE. In contrast, a single study devoted to CDs of human ABCA1 (50% sequence identity with ABCA4) expressed in *E. coli* demonstrated formation of high-MW soluble aggregates detected by dynamic light scattering [46]. It cannot be entirely excluded that structural homogeneity of recombinant ABCA4 fragments may depend on small differences in defining domain boundaries, as suggested for NBDs of some other eukaryotic ABC transporters [46, 54–57]. Another source of discrepancies could be the location and properties of purification tags. However, the heterogeneity observed in the current study was independent of the type (GST, His, Strep, 1d4) and position of such tags, whereas remarkable similarities between our results and those obtained for CDs of ABCA1 suggest that the observed abnormal conformational states could be a general artefact overlooked by the authors of studies [24–30]. Furthermore, our functional studies indicate that the apparent ATPase activity observed in samples of his-CD2-strep may at least in part originate from protein contaminants, creating another disagreement. In the earlier study devoted to the activity of CD1 of human ABCA4, detectable contaminating protein bands were attributed to proteolytic fragments of the target protein [24], whereas the image quality does not permit a reliable evaluation of protein purity in the case of CD2 [26]. Additional experiments would be required to reconcile our results with these previously published data.

Studies employing full-length ABCA4 heterologously produced in mammalian cell lines reported that this transporter localized to the endoplasmic reticulum (ER) and intracellular vesicles [19, 23, 58], raising the possibility of incomplete or incorrect folding. This prompted us to investigate the conformation of the full-length human protein transiently expressed in HEK293 cells. The choice of a transient expression system, which allows convenient production of mutated proteins, is important for future studies of disease-associated mutations. We also chose to work with ABCA4 devoid of purification tags because a case study in transgenic frogs reported mislocalization of the human protein tagged with EGFP to the inner segments of photoreceptors [59]. Selective binding to GNL agarose (Figure 7A) suggested that heterologously expressed human ABCA4 retained the predominantly high-mannose type of N-linked glycosylation found in native bovine ABCA4 [19]. Furthermore, EM analysis revealed structural homogeneity at the level of individual protein particles (Figure 7B), which were indistinguishable from those of the endogenous bovine protein. After classification and averaging of collected particles, structural features typical of native ABCA4 [31] became apparent (Figure 7C), including the elongated moiety representing the tightly interacting ECDs, the cytoplasmic region with a discernible internal cavity, and TMDs 'wrapped' in the Amphipol belt. The quality of the micrographs allows for a reliable determination of the 3D structure using very small protein amounts (unpublished results). Thus, recombinant ABCA4 expressed in mammalian cells is identical to the native protein within the resolution limits of negative stain EM. We speculate that localization of the recombinant human protein to the ER could result from the absence in the host cell of OS or an equivalent structure which could provide the specific environment found in OS disk membranes.

A recent study produced full-length human ABCA4 using a baculovirus-insect cell expression system [60]. Unlike ABCA4 expressed by us and others in mammalian cells or purified directly from bovine photoreceptors [13, 14, 17, 19, 23], this protein showed no stimulation of its ATPase activity by ATR, the proposed physiological transport substrate. A structural investigation by EM suggested that ABCA4 produced in insect cells exists predominantly in a dimeric form. It is not clear at present if this packing is physiologically relevant, although it has been suggested that a related transporter, ABCA1, may form dimers [44].

In summary, our results suggest that isolated domains of bovine ABCA4 produced in *E. coli* or yeast will require extensive optimisation to become suitable for structural studies, whereas biochemical and activity data obtained from these proteins should be interpreted with care given their structural heterogeneity and possible misfolding. Strategies to remedy the incurred problems could include co-expression of CD1 with CD2 and ECD1 with ECD2 to allow their interactions at early stages of folding and/or the use of mammalian expression systems. In contrast, the conformational identity of full-length human ABCA4 produced in mammalian cells to the bovine protein obtained from a native source opens the possibility to employ powerful recombinant DNA technology tools to further advance our understanding of structure, function and disease-related mutations of ABCA4.

Acknowledgments

FUNDING SOURCES

This work was supported by a grant from the National Institutes of Health (NIH), National Eye Institute (NEI) EY009339 (to K.P.).

We are grateful to Dr. Leslie T. Webster, Jr. for critical comments on the manuscript, to Dr. Vera Moiseenkova-Bell for assistance with the yeast expression system and to Heather Holdaway for technical assistance with EM. K.P. is John H. Hord Professor of Pharmacology.

ABBREVIATIONS

ANS	1-anilinonaphthalene-8-sulfonate
CD1 and CD2	cytoplasmic domains 1 and 2, respectively
DDM	n-dodecyl-β-D-maltopyranoside
ECD1 and ECD2	exocytoplasmic domains 1 and 2, respectively
EM	electron microscopy
NBD	nucleotide binding domain
OS	outer segment
SEC	size exclusion chromatography

References

1. Higgins CF. Annu Rev Cell Biol. 1992; 8:67–113. [PubMed: 1282354]
2. Jones PM, George AM. Cell Mol Life Sci. 2004; 61:682–699. [PubMed: 15052411]

3. Allikmets R, Singh N, Sun H, Shroyer NF, Hutchinson A, Chidambaram A, Gerrard B, Baird L, Stauffer D, Peiffer A, Rattner A, Smallwood P, Li Y, Anderson KL, Lewis RA, Nathans J, Leppert M, Dean M, Lupski JR. Nat Genet. 1997; 15:236–246. [PubMed: 9054934]
4. Weleber RG. Arch Ophthalmol. 1994; 112:752–754. [PubMed: 8002831]
5. Hamel CP. Orphanet J Rare Dis. 2007; 2:7. [PubMed: 17270046]
6. Vasiliou V, Vasiliou K, Nebert DW. Hum Genomics. 2009; 3:281–290. [PubMed: 19403462]
7. Piehler AP, Ozcurumez M, Kaminski WE. Frontiers in psychiatry / Frontiers Research Foundation. 2012; 3:17.
8. Albrecht C, Viturro E. Pflugers Arch. 2007; 453:581–589. [PubMed: 16586097]
9. Tsybovsky Y, Molday RS, Palczewski K. Adv Exp Med Biol. 2010; 703:105–125. [PubMed: 20711710]
10. Travis GH, Golczak M, Moise AR, Palczewski K. Annual review of pharmacology and toxicology. 2007; 47:469–512.
11. Palczewski K. J Biol Chem. 2012; 287:1612–1619. [PubMed: 22074921]
12. Maeda A, Golczak M, Chen Y, Okano K, Kohno H, Shiose S, Ishikawa K, Harte W, Palczewska G, Maeda T, Palczewski K. Nature chemical biology. 2012; 8:170–178.
13. Sun H, Molday RS, Nathans J. J Biol Chem. 1999; 274:8269–8281. [PubMed: 10075733]
14. Ahn J, Wong JT, Molday RS. J Biol Chem. 2000; 275:20399–20405. [PubMed: 10767284]
15. Weng J, Mata NL, Azarian SM, Tzekov RT, Birch DG, Travis GH. Cell. 1999; 98:13–23. [PubMed: 10412977]
16. Maeda A, Maeda T, Golczak M, Palczewski K. J Biol Chem. 2008; 283:26684–26693. [PubMed: 18658157]
17. Quazi F, Lenevich S, Molday RS. Nature communications. 2012; 3:925.
18. Bungert S, Molday LL, Molday RS. J Biol Chem. 2001; 276:23539–23546. [PubMed: 11320094]
19. Tsybovsky Y, Wang B, Quazi F, Molday RS, Palczewski K. Biochemistry. 2011; 50:6855–6866. [PubMed: 21721517]
20. Hozoji M, Kimura Y, Kioka N, Ueda K. J Biol Chem. 2009; 284:11293–11300. [PubMed: 19258317]
21. Ahn J, Beharry S, Molday LL, Molday RS. J Biol Chem. 2003; 278:39600–39608. [PubMed: 12888572]
22. Sun H, Nathans J. J Bioenerg Biomembr. 2001; 33:523–530. [PubMed: 11804194]
23. Sun H, Smallwood PM, Nathans J. Nat Genet. 2000; 26:242–246. [PubMed: 11017087]
24. Biswas EE. Biochemistry. 2001; 40:8181–8187. [PubMed: 11444963]
25. Biswas EE, Biswas SB. Biochemistry. 2000; 39:15879–15886. [PubMed: 11123914]
26. Biswas-Fiss EE. Biochemistry. 2003; 42:10683–10696. [PubMed: 12962493]
27. Biswas-Fiss EE. Biochemistry. 2006; 45:3813–3823. [PubMed: 16533065]
28. Biswas-Fiss EE, Kurpad DS, Joshi K, Biswas SB. J Biol Chem. 2010; 285:19372–19383. [PubMed: 20404325]
29. Suarez T, Biswas SB, Biswas EE. J Biol Chem. 2002; 277:21759–21767. [PubMed: 11919200]
30. Biswas-Fiss EE, Affet S, Ha M, Biswas SB. J Biol Chem. 2012; 287:44097–44107. [PubMed: 23144455]
31. Tsybovsky Y, Orban T, Molday RS, Taylor D, Palczewski K. Structure. 2013; 21:854–860. [PubMed: 23562398]
32. Figler RA, Omote H, Nakamoto RK, Al-Shawi MK. Archives of biochemistry and biophysics. 2000; 376:34–46. [PubMed: 10729188]
33. Moiseenkova-Bell VY, Stanciu Serysheva LA II, Tobe BJ, Wensel TG. Proc Natl Acad Sci U S A. 2008; 105:7451–7455. [PubMed: 18490661]
34. Moiseenkova VY, Hellmich HL, Christensen BN. Biochem Biophys Res Commun. 2003; 310:196–201. [PubMed: 14511670]
35. Illing M, Molday LL, Molday RS. J Biol Chem. 1997; 272:10303–10310. [PubMed: 9092582]

36. Tang G, Peng L, Baldwin PR, Mann DS, Jiang W, Rees I, Ludtke SJ. Journal of structural biology. 2007; 157:38–46. [PubMed: 16859925]
37. Frank J, Radermacher M, Penczek P, Zhu J, Li Y, Ladjadj M, Leith A. Journal of structural biology. 1996; 116:190–199. [PubMed: 8742743]
38. Penczek PA, Zhu J, Frank J. Ultramicroscopy. 1996; 63:205–218. [PubMed: 8921628]
39. Sievers F, Wilm A, Dineen D, Gibson TJ, Karplus K, Li W, Lopez R, McWilliam H, Remmert M, Soding J, Thompson JD, Higgins DG. Molecular systems biology. 2011; 7:539. [PubMed: 21988835]
40. Vahedi-Faridi A, Jastrzebska B, Palczewski K, Engel A. Microscopy (Oxf). 2013; 62:95–107. [PubMed: 23267047]
41. Popot JL, Althoff T, Bagnard D, Baneres JL, Bazzacco P, Billon-Denis E, Catoire LJ, Champeil P, Charvolin D, Cocco MJ, Cremel G, Dahmane T, de la Maza LM, Ebel C, Gabel F, Giusti F, Gohon Y, Goormaghtigh E, Guittet E, Kleinschmidt JH, Kuhlbrandt W, Le Bon C, Martinez KL, Picard M, Pucci B, Sachs JN, Tribet C, van Heijenoort C, Wien F, Zito F, Zoonens M. Annual review of biophysics. 2011; 40:379–408.
42. Coleman JA, Quazi F, Molday RS. Biochim Biophys Acta. 2013; 1831:555–574. [PubMed: 23103747]
43. Quazi F, Molday RS. Essays in biochemistry. 2011; 50:265–290. [PubMed: 21967062]
44. Nagata KO, Nakada C, Kasai RS, Kusumi A, Ueda K. Proc Natl Acad Sci U S A. 2013; 110:5034–5039. [PubMed: 23479619]
45. Sorrenson B, Suetani RJ, Williams MJ, Bickley VM, George PM, Jones GT, McCormick SP. J Lipid Res. 2013; 54:55–62. [PubMed: 23087442]
46. Roosbeek S, Caster H, Liu QZ, Berne PF, Duverger N, Christiaens B, Vandekerckhove J, Peelman F, Labeur C, Rosseneu M. Protein expression and purification. 2004; 35:102–110. [PubMed: 15039072]
47. Martsev SP, Chumanevich AA, Vlasov AP, Dubnovitsky AP, Tsybovsky YI, Deyev SM, Cozzi A, Arosio P, Kravchuk ZI. Biochemistry. 2000; 39:8047–8057. [PubMed: 10891087]
48. Martsev SP, Dubnovitsky AP, Stremovsky OA, Chumanevich AA, Tsybovsky YI, Kravchuk ZI, Deyev SM. FEBS Lett. 2002; 518:177–182. [PubMed: 11997042]
49. Tsybovsky YI, Shubenok DV, Stremovskiy OA, Deyev SM, Martsev SP. Biochemistry Biokhimiia. 2004; 69:939–948. [PubMed: 15521808]
50. Shubenok DV, Tsybovsky YI, Stremovskiy OA, Deyev SM, Martsev SP. Biochemistry Biokhimiia. 2009; 74:672–680. [PubMed: 19645673]
51. Papermaster DS, Reilly P, Schneider BG. Vision Res. 1982; 22:1417–1428. [PubMed: 6985105]
52. Papermaster DS, Schneider BG, Zorn MA, Kraehenbuhl JP. J Cell Biol. 1978; 78:415–425. [PubMed: 690173]
53. Mitra N, Sinha S, Ramya TN, Surolia A. Trends Biochem Sci. 2006; 31:156–163. [PubMed: 16473013]
54. Duffieux F, Annereau JP, Boucher J, Miclet E, Pamlard O, Schneider M, Stoven V, Lallemand JY. European journal of biochemistry / FEBS. 2000; 267:5306–5312. [PubMed: 10951189]
55. Gentzsch M, Aleksandrov A, Aleksandrov L, Riordan JR. The Biochemical journal. 2002; 366:541–548. [PubMed: 12020354]
56. Kerr ID, Berridge G, Linton KJ, Higgins CF, Callaghan R. European biophysics journal: EBJ. 2003; 32:644–654. [PubMed: 12830334]
57. Wang C, Castro AF, Wilkes DM, Altenberg GA. The Biochemical journal. 1999; 338(Pt 1):77–81. [PubMed: 9931301]
58. Zhong M, Molday LL, Molday RS. J Biol Chem. 2009; 284:3640–3649. [PubMed: 19056738]
59. Wiszniewski W, Zaremba CM, Yatsenko AN, Jamrich M, Wensel TG, Lewis RA, Lupski JR. Hum Mol Genet. 2005; 14:2769–2778. [PubMed: 16103129]
60. Pollock NL, McDevitt CA, Collins R, Niesten PH, Prince S, Kerr ID, Ford RC, Callaghan R. Biochim Biophys Acta. 2014; 1838:134–147. [PubMed: 24036079]

- Full-length ABCA4 transporter was expressed in mammalian cells
- Individual soluble fragments of ABCA4 were produced in bacteria and yeast
- Individual ABCA4 domains form oligomers cross-linked with disulfide bonds
- Recombinant ABCA4 is structurally equivalent to ABCA4 purified from a native source

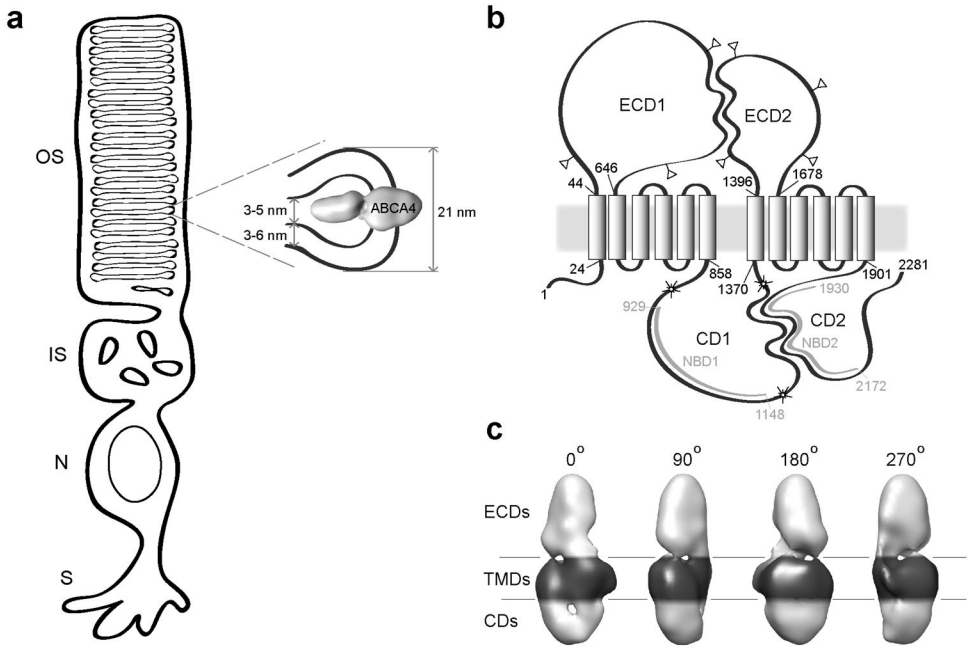

Figure 1.

a, schematic representation of a rod photoreceptor cell. OS: outer segment; IS: inner segment; N: nucleus; S: synaptic ending. ABCA4 is localized to the rims of disk membranes populating OS. Geometrical parameters of the disk rim are from (*61*). *b*, topological model of bovine ABCA4. Transmembrane helices are shown as cylinders. Numbers indicate approximate boundaries of domains. NBDs 1 and 2 are shown within cytoplasmic domains (CDs) 1 and 2. Glycosylation and phosphorylation sites are marked with triangles and stars, respectively (three phosphorylation sites clustered at the end of CD1 (*19*) are shown as a single star). ECD: exocytoplasmic domain. *c*, angular views of the 18 Å-resolution structure of native bovine ABCA4 (*31*). The position of the lipid bilayer is shown with lines. TMDs are colored black.

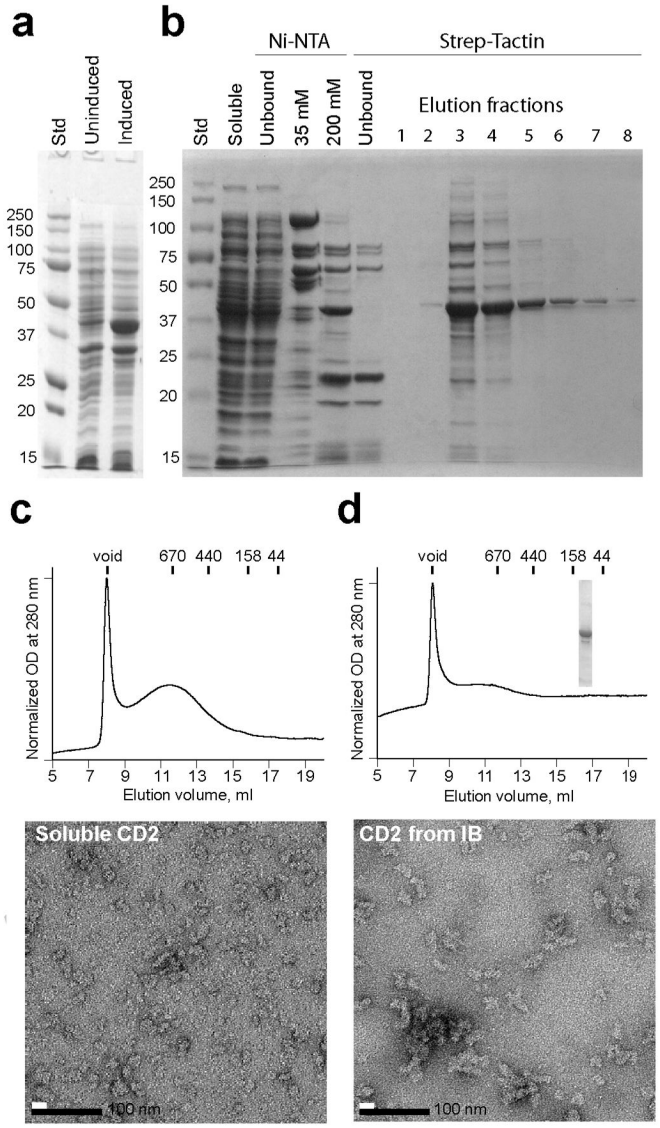

Figure 2.

Purification and properties of CD2. *a*, expression of his-CD2-strep in *E. coli* BL21 Star (DE3). The target protein band with an apparent MW of 40 kDa is observed after induction with IPTG. *b*, Coomassie-stained SDS-PAGE gel illustrating the two-step purification method. “35 mM” and “200 mM” refer to the concentration of imidazole. *c* and *d*, SEC profiles (top) and EM micrographs (bottom) of his-CD2-strep obtained from soluble and insoluble fractions of cell lysate, respectively. Inset in panel *d* shows SDS-PAGE result for purified his-CD2-strep. Numbers (in kDa) above chromatograms indicate positions of calibration peaks. White bars on the micrographs correspond to the longest dimension (20 nm) of native full-length ABCA4 under identical conditions (*31*).

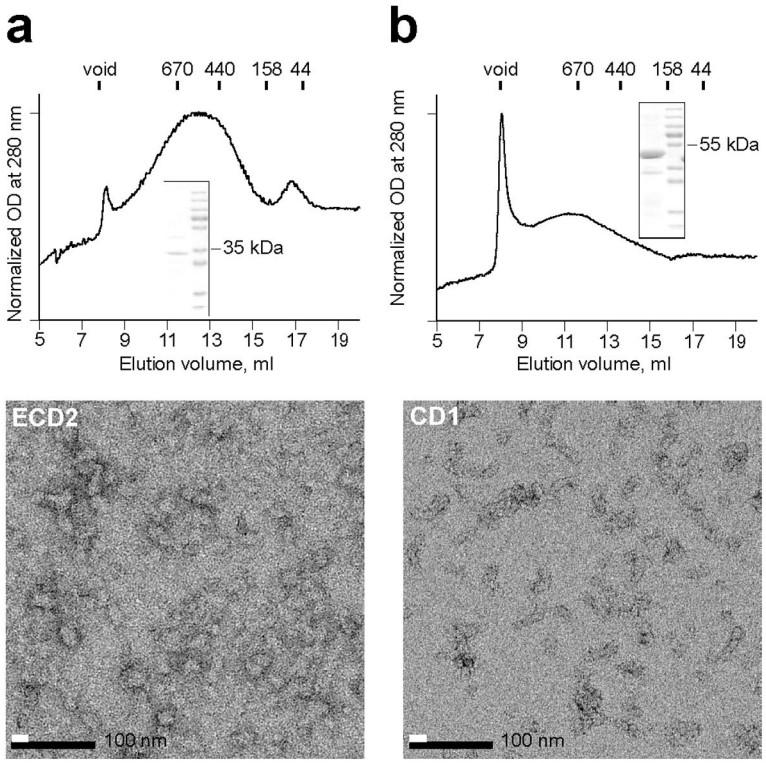

Figure 3.

ECD2 and CD1 form non-specific oligomers. SEC profiles (top) and EM micrographs (bottom) of his-ECD2 (*a*) and his-CD1 (*b*) refolded from bacterial IB. Numbers (in kDa) above chromatograms indicate positions of calibration peaks. Insets show SDS-PAGE results for purified fragments. White bars on the micrographs correspond to the longest dimension (20 nm) of native full-length ABCA4 under identical conditions (*31*).

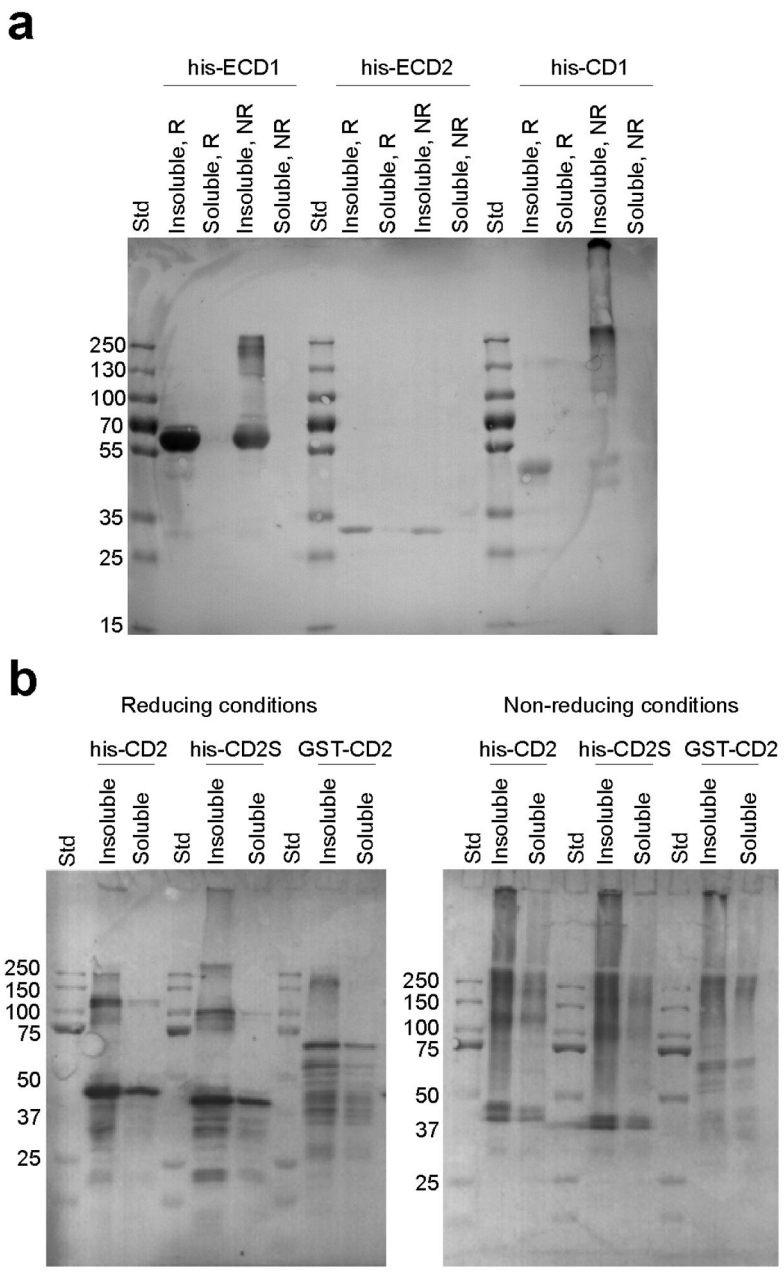

Figure 4.

Recombinant ABCA4 domains expressed in *E. coli* form non-specific inter- and intra-molecular disulphide bonds. *a*, total lysates of cells expressing his-ECD1, his-ECD2 and his-CD1 separated by SDS-PAGE in reducing (R) and non-reducing (NR) conditions. ABCA4 domains were detected by Western blot using an anti-His tag monoclonal antibody. *b*, total lysates of cells expressing three variants of CD2 separated by SDS-PAGE in reducing and non-reducing conditions. his-CD2s: his-CD2short. CD2 was detected by Western blot using the monoclonal Rim3F4 antibody specific to ABCA4 (*35*). High MW bands and smears can be observed in the absence of the reducing agent (DTT), whereas the monomer fraction is

significantly reduced. In the case of his-CD1 and his-CD2 constructs, the non-reduced monomer is represented by more than one band.

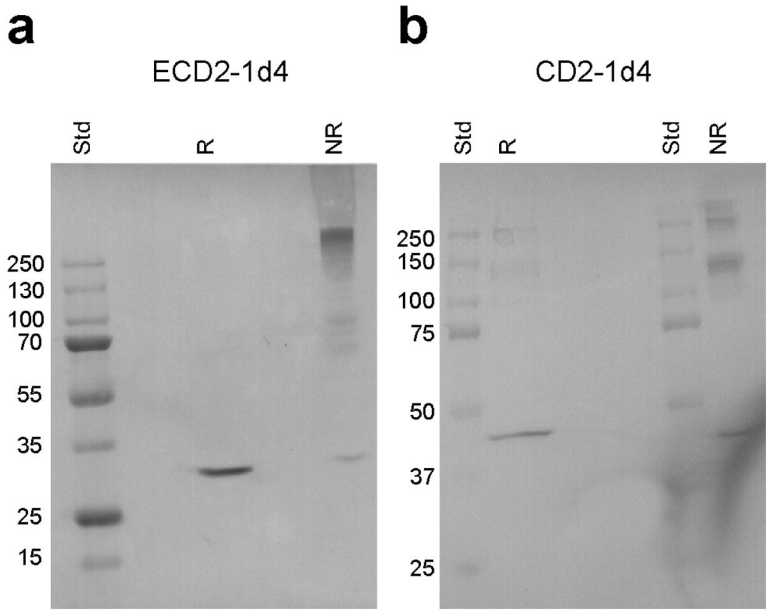

Figure 5.

ECD2 and CD2 domains expressed in yeast form non-specific inter-molecular disulphide bonds. Soluble fractions of yeast cells expressing ECD2-1d4 (*a*) and CD2-1d4 (*b*) separated by SDS-PAGE in reducing (R) and non-reducing (NR) conditions. ABCA4 fragments were detected by Western blot using the 1d4 monoclonal antibody.

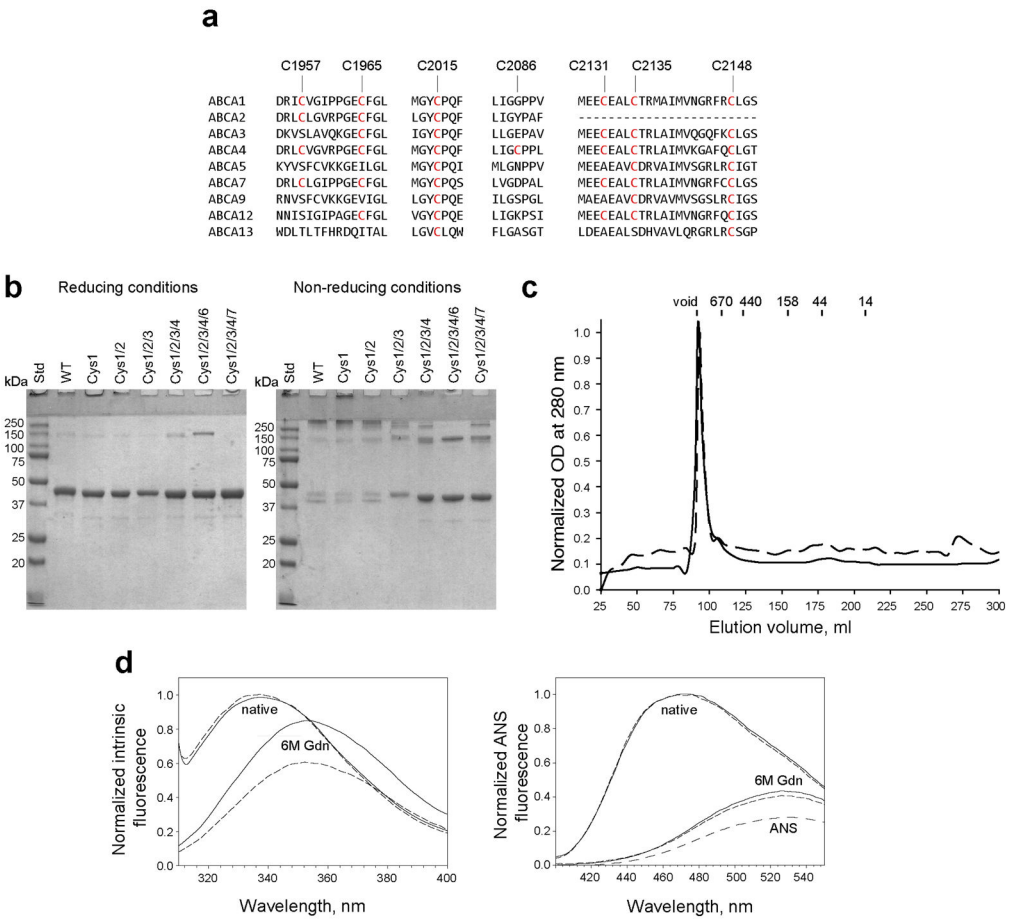

Figure 6.

Role of Cys residues in folding and non-specific oligomerization of CD2. *a*, conservation of Cys residues in CD2 of bovine ABCA family members with available amino acid sequences. Seven ABCA4 Cys residues are marked on top. *b*, SDS-PAGE analysis in reducing (left) and non-reducing (right) conditions of purified his-CD2 variants with increasing numbers of Cys residues replaced with Ser. The gels were stained with Coomassie Brilliant Blue. The replaced Cys residues are indicated above each lane and numbered as follows. Cys1: 1957; Cys2: 1965; Cys3: 2015; Cys4: 2086; Cys5: 2135; Cys6: 2148; Cys7: 2131. Replacement of Cys alleviates the chemical heterogeneity of his-CD2. *c*, SEC of wild type his-CD2 (solid line) and the Cys 1/2/3/4/6 mutant (dashed line) on Sephacryl S-300 (matrix exclusion limit 1.5 MDa). Numbers (in kDa) above chromatograms indicate positions of calibration peaks. *d*, intrinsic tryptophan (left) and ANS (right) fluorescence spectra of purified, refolded WT his-CD2 (solid line) and the Cys 1/2/3/4/6 mutant (dashed line) under native conditions (‘native’) and in the presence of 6 M Gdn (‘6M Gdn’). A fluorescence spectrum of free ANS (‘ANS’) is shown for comparison.

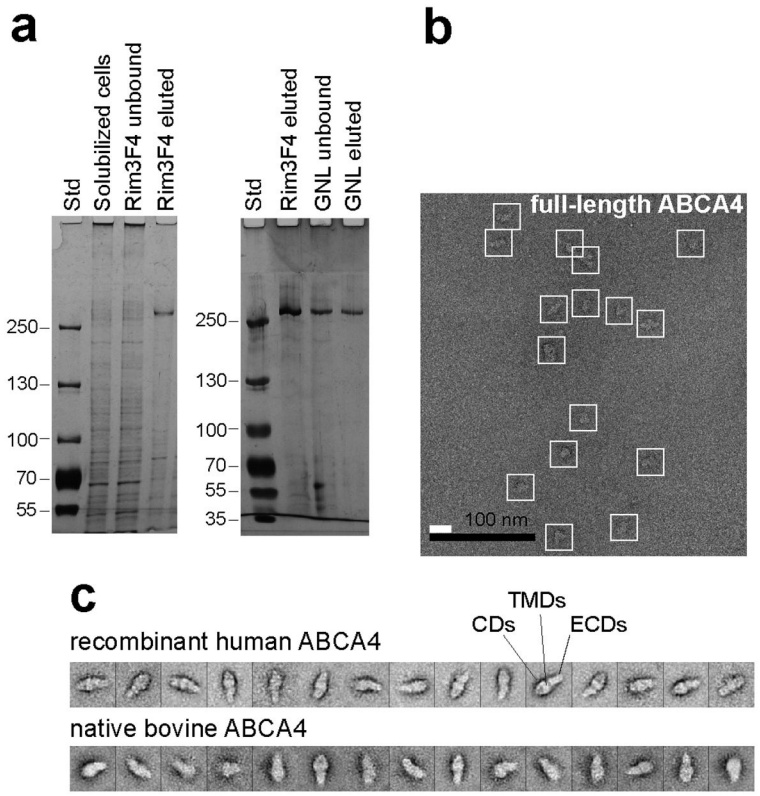

Figure 7.

Purification and properties of full-length human ABCA4 expressed in HEK293 cells. *a*, silver-stained SDS-PAGE gels illustrating purification of ABCA4 using the agarose-conjugated Rim3F4 monoclonal antibody only (left) and the combination of the previous step with agarose-conjugated *Galanthus nivalis* lectin (GNL) (right). See Materials and Methods for details. *b*, an EM micrograph of uranyl acetate-stained human recombinant ABCA4. Individual ABCA4 particles are shown in white boxes. *C*, examples of 2D class averages for human recombinant ABCA4 (top) and the native bovine protein (bottom). Positions of CDs, TMDs and ECDs are indicated for one class.

Table 1

Bovine ABCA4 fragments expressed in *E. coli* and *S. cerevisiae*.

Construct	Fragment	Soluble expression[a]	After refolding
		E. coli	
his-ECD1	44–646	Low	Insoluble
his-ECD2	1396–1678	Low	Soluble
his-CD1	919–1284	Low	Soluble
his-CD2short	1904–2262	Significant	Soluble
his-CD2		Significant	Soluble
his-CD2-strep	1904–2281	Significant	Soluble
GST-CD2		Significant	N/A
his-NBD2	1931–2172	No	Insoluble
		S. cerevisiae	
ECD2-1d4	1396–1678	N/A	N/A
CD2-1d4	1904–2281	N/A	N/A

[a]The level of expression in the soluble fraction was assigned as follows. Low: expression was detected by WB but one-step Ni-NTA purification did not produce a dominant band of expected MW as determined by Coomassie-stained SDS-PAGE. Significant: one-step Ni-NTA purification produced a dominant band of expected MW as determined by SDS-PAGE. N/A: not analyzed.